Interlocking Vaults by Voronoi Decomposition of 3D Space

Neeraj Yadav[1]

[1]Department of Architecture, Texas A&M University, College Station; nyadavemail@gmail.com

Abstract

Aided by advancements in computation and fabrication techniques, this paper introduces a novel method to create assemblies by Voronoi decomposition of 3D space. The scope of this paper is limited to the generation of interlocking modules to constitute arches and vaults. Every module is generated in tandem with adjacent modules and is assured to be an exact fit, independent of the intent to have repetitive or non-repetitive modules.

Introduction

Interlocking patterns are widely found in nature and have been a fascination of architects and engineers throughout history. From early post-and-lintel system of Stonehenge to traditional Japanese woodwork and beyond, there are numerous structures that are testaments to the continuous involvement and body of work that has gone into interlocking structures. While every generation has their own techniques and methods, the current advancements in graphics and visualization along with innovations and affordability in manufacturing are bringing the dawn of a new phase in architecture and construction.

The role of geometry is fundamental to developing sound interlocking structures. Rene Descartes introduced analytical geometry and illustrated a theory in the third part of his *Principia Philosophiae*, published in 1644, to demonstrate the universe as set of (weighted) regions around each star-the "*heavens*" with help of a Vortices diagram [1]. This introduced the notion of dividing space in spheres' of influence. It was much later in 1850 that Peter Gustav Lejeune Dirichlet provided a mathematical formulation on influence of point p on another point q for R^2 and R^3 vector space [2] while it was in 1908 that Georges Feodosovic Voronoi provided the formulation for R^n vector space [3].

Voronoi tessellation has featured heavily in research and arts over the last few decades. However, the application to interlocking structures and interlocking form-finding have been limited so far. Prior studies have already recognized and assessed that the role of geometry and tessellations is instrumental in understanding and developing topological interlocking systems [4]. Joseph Abellie' and Sébastien Truchet' interlocking flat vaults and their extensions to barrel vaults feature prominently due to the innovative use of repetitive configurations [5]. Now, methods and tools are required to utilize Dirichlet Voronoi tessellation, or Voronoi tessellation as it is widely known as, in relation to interlocking structures. A recent paper discussed the use of 2D Voronoi tessellation after decomposing curves into points and create space-filling structures [6]. This provided an interesting opportunity to explore Voronoi decomposition of 3D space based on curves in order to generate arch and vault assemblies. Meanwhile, another in-press manuscript explores the generation of Abellie Tiles based on fabric symmetries using 3D Voronoi tessellation [7].

The initial research objective was to develop a tool to explore the possibility of generating interlocking arch using curves decomposed to points and their subsequent Voronoi computation. The critical challenge in doing so is determining the bounding geometry for the Voronoi cells while ensuring the absence of any overlap or unintended break in the module and arch form. On receiving positive results, the scope was extended to vault structures. A 7-module arch prototype was fabricated using additive manufacturing to test practicality of a simple interlocking mechanism. This paper presents the method and findings to further explore interlocking geometry in architecture and construction.

Methodology

The novelty of the presented method is two-fold. Firstly, regarding the boundary determination for the Voronoi decomposition and secondly, regarding the flexible count of unique modules required to complete an arch or vault structure. Figure 1 displays, with the help of a semicircular barrel vault, the coordinates system and terminology followed in this paper.

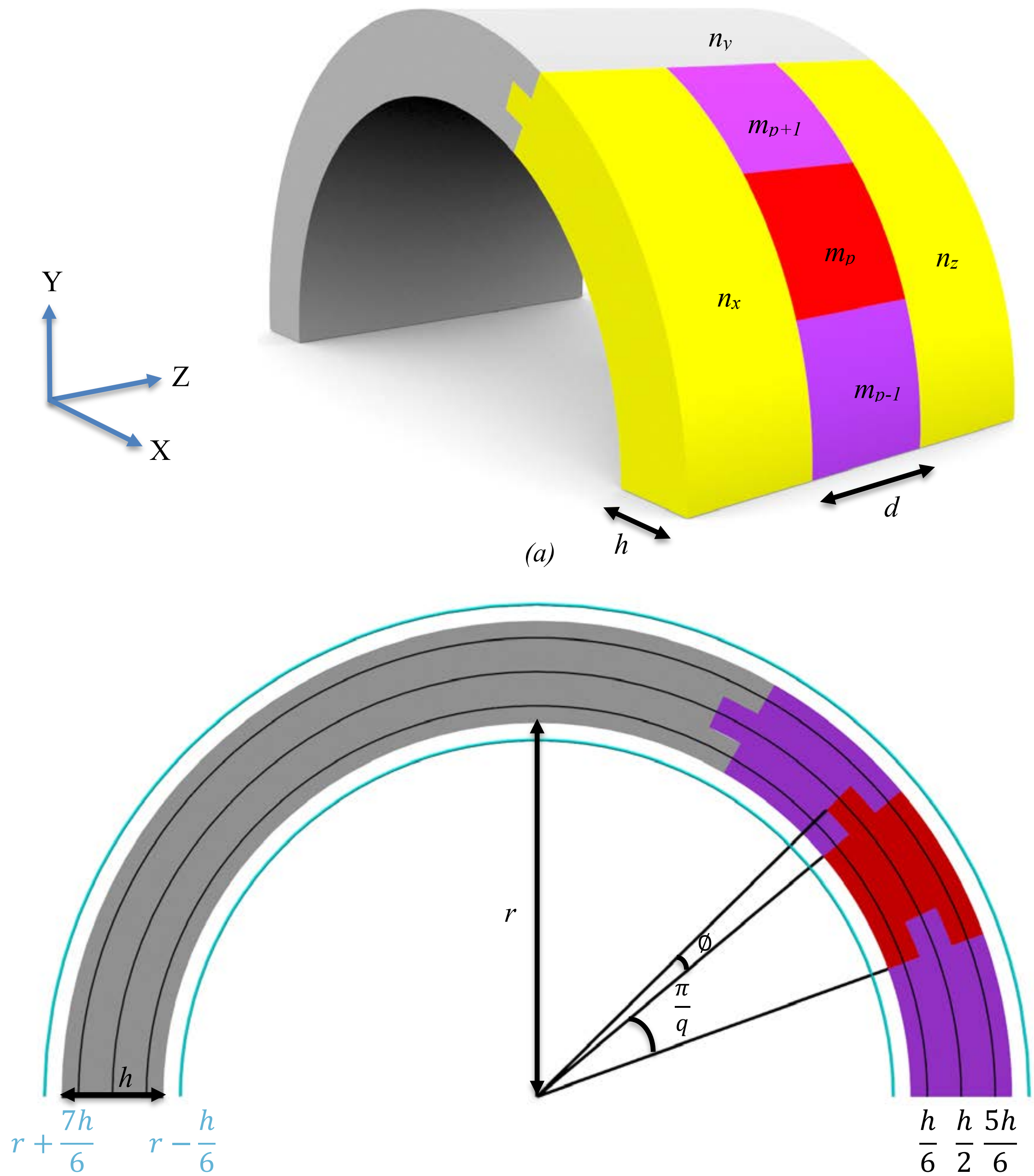

Figure 1: *The coordinate system along with the key parameters of the vault assembly are depicted in (a) while additional parameters are showcased at* $\frac{d}{2}$ *cross-section in (b).*

The overall logic behind the methodology is explained with a 12-step process for a semi-circular barrel vault. Step 1 introduces the fundamentals and terminology while Step 2-6 details the procedure to generate the curves in 3D Space. The decomposition of the curves is detailed in Step 7-12 to determine the seed point collection and neighboring boundary point collection required for 3D Voronoi cell computation.

1. The overall vault structure is considered a linear assembly of *n* arches with *d* depth, *r* rise and *h* cross-section height, where *n* can take any integer value greater than 1, and *d*, *r* and *h* are positive real number as shown in Figure 1a. Length *l* of vault is a scalar function of *n* and *d.*
2. The cross-section of an arch n_y at $\frac{d}{2}$ is divided using three arcs at $\frac{h}{6}$, $\frac{h}{2}$ and $\frac{5h}{6}$. The innermost and outermost arcs form the guide arcs while the center arc forms the interlock arc providing interlocking in XY plane.
3. Both guide arcs are further divided into *q* curves representing *m* modules such that each curve forms an angle of $\frac{\pi}{q}$ at the center. While *q* can take any integer value greater than 1, only odd integers were assigned to ensures the presence of a keystone and avoid an interlocking plane at the center of the arch. See Figure 1b for representation.
4. The interlock arc is also divided into *q* curves; however, they are offset by an interlock angle ø, where $\frac{\pi}{q} > ø > 0$, toward the keystone curve and this results in shorting of keystone interlock curve by 2ø $(r + \frac{h}{2})$.
5. All guide curves and the keystone interlock curve are replicated and translated to $\frac{d}{4}$ and $\frac{3d}{4}$.
6. All interlock curves except the keystone interlock curve are replicated and translated to $\frac{3d}{4}$ and *d* to provide interlocking in Z direction.
7. A total of *q* modules with a set of 9 curves each are identified, and one such set, m_p, where $q \geq p > 0$ and *p* takes integer values, is selected and decomposed into *i* points. All endpoints are excluded to avoid any intersection with neighboring modules. Hence, *i* can take any integer value greater than 2. Rest of the points 9*(i-2) form the seed point collection s_p for the Voronoi computation of module *p*. A curve set m_p is represented with red color in Figure 2.
8. A Module bound is constituted by similar decomposition of m_{p-1} and m_{p+1} curve set to *i* points and excluding the endpoints from the collection. Total points in module bound is 2*9*(i – 2).
9. An arch bound is constituted by n_x and n_z arches which can be obtained by translating decomposed m_{p-1}, m_p and m_{p+1} of n_y arch by – d and d. Total points in arch bound is 6*9*(i-2).
10. An inner and outer vault bound is created by decomposition of arch curve with rise $(r - \frac{h}{6})$ and $(r + \frac{7h}{6})$ respectively into *j* points each and offsetting it to $\frac{d}{4}$ and $\frac{3d}{4}$. Total points in vault bound is 2*3**j*. Here j can take any positive integer value and will accordingly impact the internal and external form of the module.
11. The point collection consisting module bound, arch bound and vault bound serves as the bounding points b_p for the Voronoi computation of module *p*. Upon computation of the Voronoi cells for s_p with b_p as neighboring points, the union of the 3D Voronoi cells will manifest into module *p*. If desired, before taking the union, the generated form can be transformed to a porous module by scaling the cell by a factor *f*, 0.5 for this study, offsetting the scaled faces and extruding them using vector joining the face center and Voronoi cell center. Later, a union of scaled extruded faces can be subtracted from union of original cells to obtain porous modules. Later, Catmull-Clark subdivision [9] can be used for smoothening keeping the corners fixed.
12. The keystone module can be obtained by repeating step 7-11. Rest of the modules can be substituted by translations of module *p* in a semi-circular vault. Otherwise, every module can be individually generated especially if the design intent is to have non-repetitive and symmetric vault structure or non-repetitive and non-symmetric vault structure.

The bounding point collection referred as b_p is visualized in Figure 2 below. The complete b_p set, for i = 6 and j =100, contains 888 points while the m_p set of curves will be sampled to 36 points and form the seed point collection s_p.

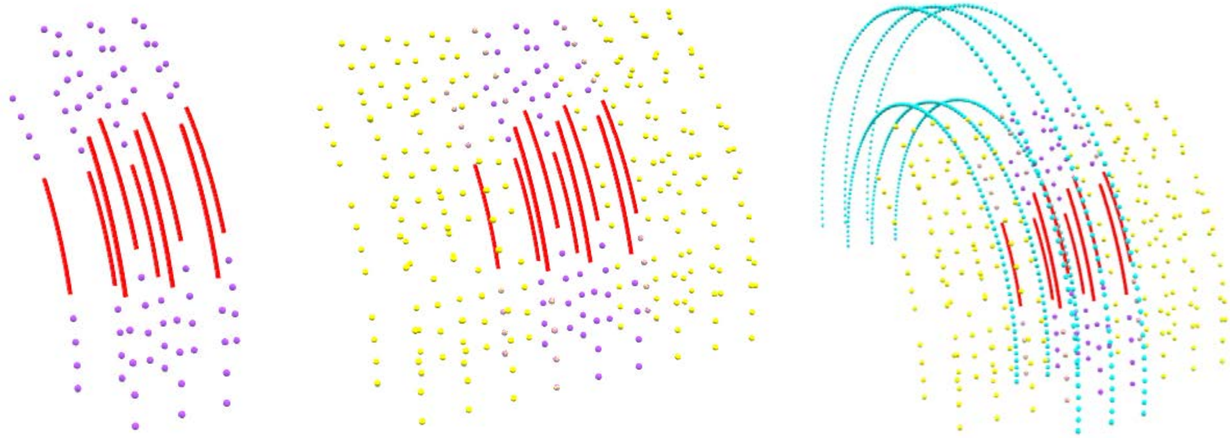

(a) (b) (c)

Figure 2: *(a) Red curves are representative of 9 curves, three arcs each at $\frac{h}{6}$, $\frac{h}{2}$ and $\frac{5h}{6}$, that together constitute the m_p set. 72 purple colored points represent the module bound after decomposing the m_{p-1} and m_{p+1} curve set into 6 points each (i = 6) and removing the endpoints. In addition to the module bound and m_p set, (b) shows the arch bound displayed in yellow color. The seed point collection s_p and the module bound is translated to n_x and n_z arches for a total of 216 points (i = 6). Subfigure (c) depicts the vault bound (j = 100) for a total of 600 points in cyan color along with the module bound and arch bound.*

The rendering of the module formed by the m_p set of curves is featured in Figure 3 corresponding to Step 11 in the aforementioned methodology. The conversion of the module obtained by Voronoi decomposition to a porous module is carried out to reduce the weight of the module. If Catmull-Clark subdivision is applied, the corners of the input module should be set to fixed. However, any severe shrinking should be avoided while some minor shrinking can be help offset manufacturing deviations.

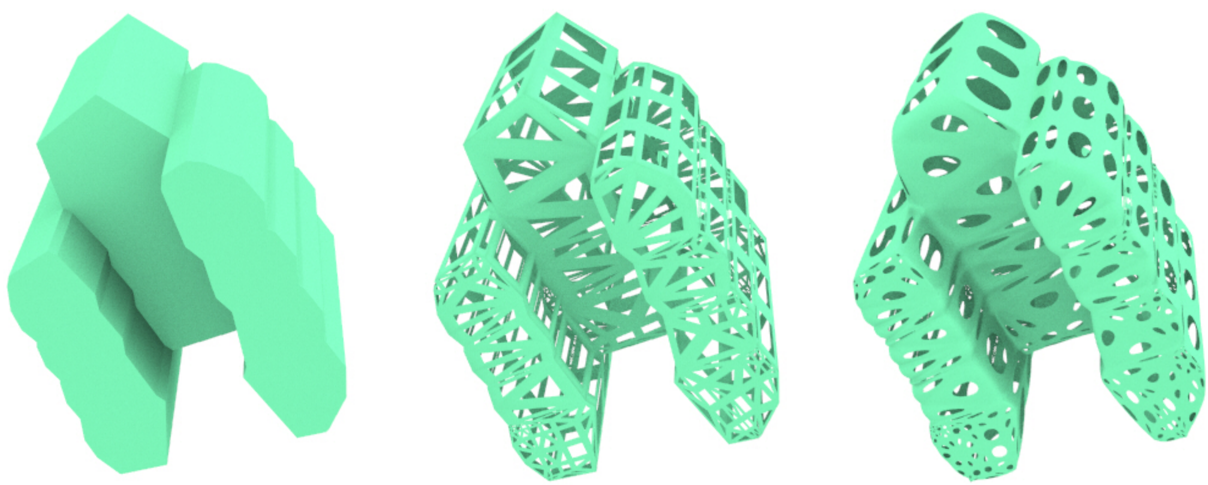

(a) (b) (c)

Figure 3: *(a) Module m_2 resulting from the curve and bounding point collection b_p shown in Figure 2; (b) Porous version of module m_2; (c) Module m_2 after Catmull-Clark subdivision while keeping the corners fixed.*

The complete vault assembly from the resulting module in Figure 3c is shown in Figure 4a. The vault assembly consists of two arch (n = 2) and nine modules each (q = 9). The module m_2, obtained in Figure 3c, can be translated to replace all other modules except the keystone modules m_5. The keystone module is generated following the same process with m_5 curve set. The resulting arch is translated by *depth (d = 3)* to obtain a vault comprised of two arches. Figure 4b displays a symmetric vault where all nine modules are generated individually, and seven arches have been assembled together (n = 7). This setup requires 5 unique modules to continue in either direction.

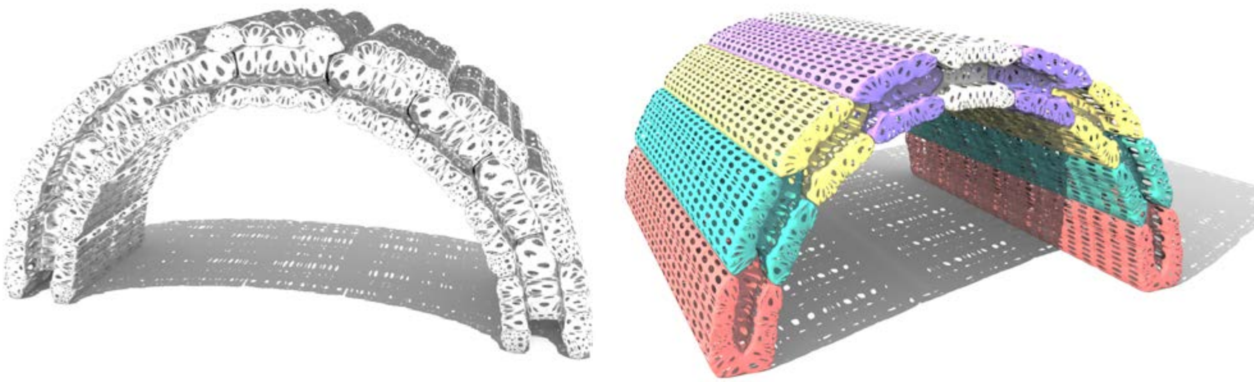

Figure 4: *(a) Semicircular barrel vault assembly of two arches after generating the keystone module m_5 and translations of side module m_2 for a total of 2 unique modules. (b) A semi-circular symmetric interlocking vault involving 5 unique modules that can be repeated to continue the assembly in Z direction. {Parameters: n = 2 (a); n = 7 (b), d = 3, r = 7, h = 2, q = 9, ø = 5º, i = 10, j = 100}*

All the demonstrated designs were generated using the proposed method in Rhinoceros 3D and Grasshopper interface by McNeel and Associates version 6 SR16 [8]. The decomposition of curves and Voronoi computation was carried out using Grasshopper nodes. A screenshot of the algorithm is presented in Figure 5.

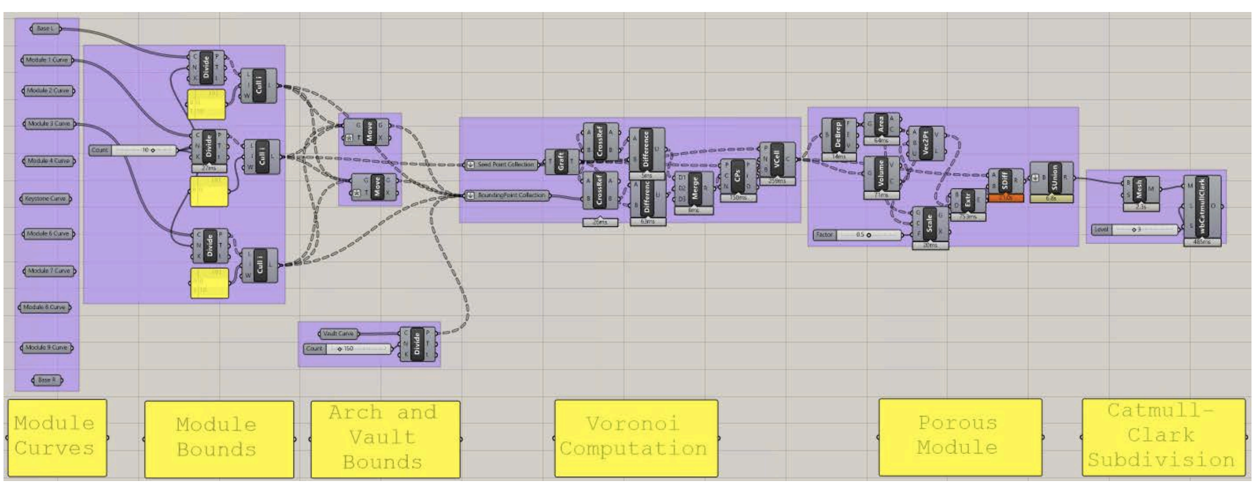

Figure 5: *Generic Template for Rhinoceros3D-Grasshopper algorithm.*

While all mentioned parameters are crucial in determining the form of the interlocking modules, the impact of inner and outer vault bound curves and their subsequent sampling to points is of significant prominence in the visual appeal of the arch or vault structure. Figure 6 shows the impact of points contained in the vault bound on the form. The protrusions result from the low j count. Since the vault bound curves are decomposed into fewer points, the seed point collection's influence increases towards the inside as well as the outside vault bound. For this figure, the inner as well as the outer bound curves were decomposed into 17 points. As a result of that, 16 protrusions can be noticed filling the space between the bounding point collection on the inside and outside as determined by Voronoi tessellation.

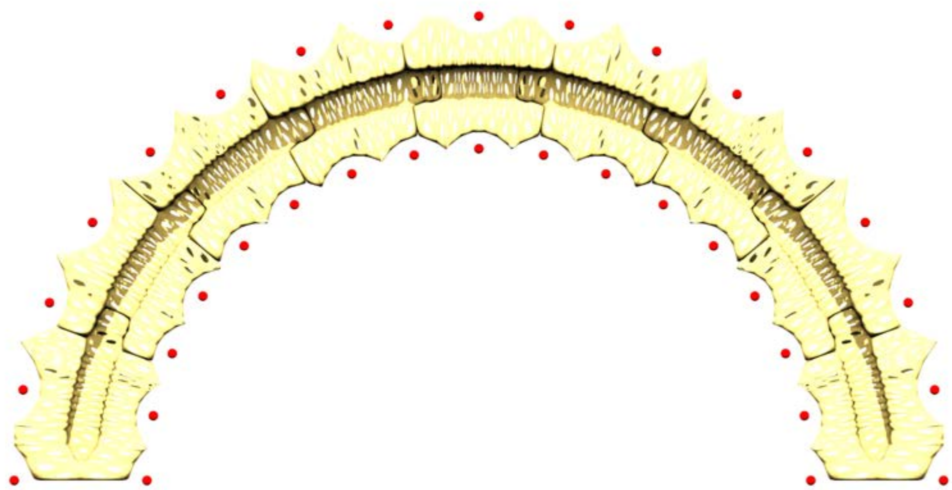

Figure 6: *Front view of an arch showing large protrusion resulting from sampling of vault bound curves to relatively less points. {Parameters: n = 1, d = 3, r = 7, h = 2, q = 9, ø = 5º, i = 10, and j = 17}*

Similarly, if *j* count is reduced even further, the protrusion become more pronounced in the internal as well as external form of the arch or vault structure. Figure 7 displays a non-repetitive symmetric vault where the impact of both *i* and *j* is be visualized. The bottom two modules on either side are kept in their non-porous state while the top three modules have been processed to create porous modules and smoothened using Catmull-Clark subdivision.

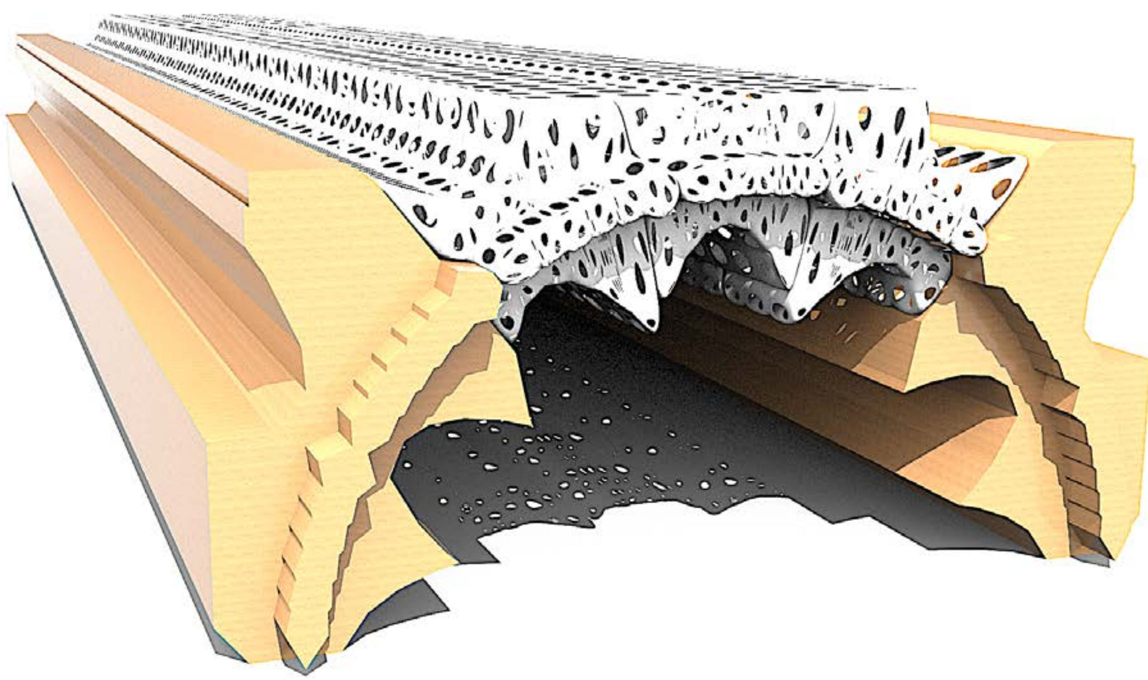

Figure 7: *Vault Bound count resulting in protrusions, interior count 7. {Parameters: n = 12, d = 3, r = 7, h = 2, q = 9, ø = 3º, i = 8, and j = 7}*

Fabrication and Assembly

The modules can be manufactured with traditional injection molding or casting method if the original module is not transformed to a porous module, otherwise, it might be extremely challenging to manufacture them. However, with enhanced feasibility and availability of additive manufacturing, the prototypes can be printed before manufacturing full-scale assemblies. The build plate of available 3D printer should be considered while determining the module size and count of arch or vault structure. Also, in case of additive manufacturing of porous structure, the user needs to recognize if the printing process will require supports. The removal of supports can be extremely challenging if not well throughout beforehand, one alternate is to use water soluble support like polyvinyl alcohol (PVA).

Figure 8 displays one arch prototype that was printed using Fused Deposition Modeling (FDM) with polylactic acid (PLA) on Ender3 3D Printer [10]. The module form was populated with 250 points to generate the internal Voronoi tessellation and was printed without much support structure except for the interlocking extrusions. The PLA supports were broken off before the assembly. The slicing of the computer-aided model was carried out in Ultimaker Cura 4.2.1 [11]. The print settings are as follows: Infill = 20 %, Layer Height = 0.12 mm, Speed 50 mm/s, Bed Temperature = 60 ºC, and Print Temperature = 211 ºC. The model parameters were {n = 1, d = 2, r = 6, h = 2, q = 7, ø = 5º, i = 15, and j = 200}.

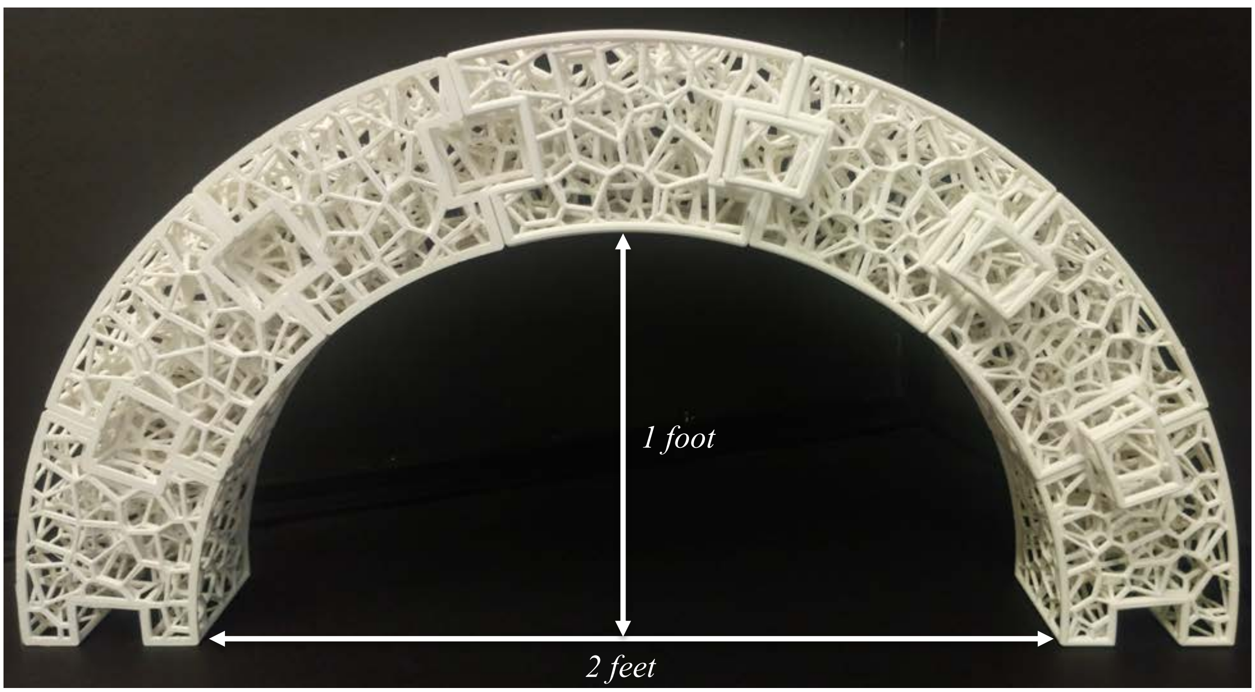

Figure 8: An additively manufactured assembly of a 7 module semi-circular arch (1 keystone and 6 repetitive side modules) with 1 foot rise and 2 feet span.

It is worth noting that the interlocking curve is significantly shorter than the guide curves and has a direction associated to it such that arch will interlock horizontally on both sides. The volume generation of the arch in Figure 8 was obtained by thickening of the outer edges of the module and the edges of the internal Voronoi cells to cylindrical pipes. This can be challenging especially for interlocking assemblies since that might result in overlap of modules. Hence, Step 11 was introduced in the methodology to ensure that the volume and thickness of elements in the module can be determined with the scaling factor f (0.5 for this study) to avoid any overlap possibilities while creating porous modules.

The arch is assembled using horizontal translations along the Z axis. This include the keystone module placement which is traditionally placed at the end with a vertical Y direction movement. Shown in Figure 9 is the exploded view of a nine module arch requiring a horizontal movement to interlocking with the adjacent modules as well as the next arch.

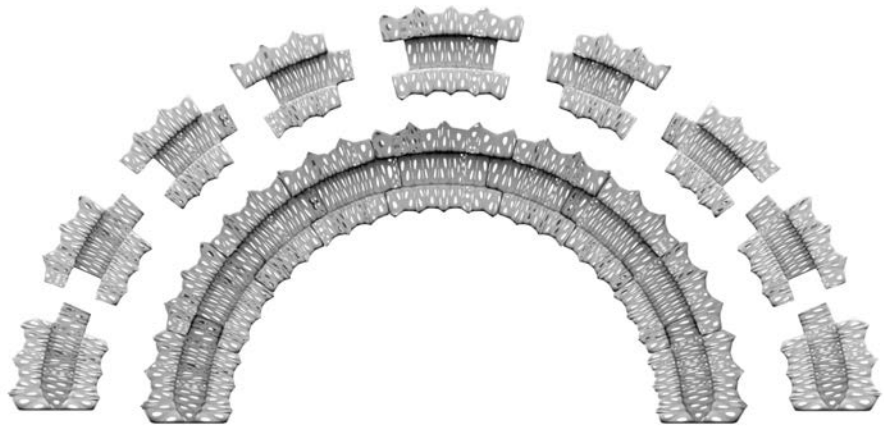

Figure 9: *An exploded view of a nine module semi-circular arch with 3 unique modules.*

Anchoring End Modules

Arches and vaults tend to flatten out under gravity and generally require supports at the ends. If left unsupported, it is unlikely that the vault will stay in place. The stability of the design presented in Figure 8 is mainly due to the light weight of the arch as well as the relatively large depth d and cross-section height h parameters as compared to the scale of the arch itself. However, if the two parameters are reduced without adjusting the scale of the arch, it will likely require anchoring the end modules to maintain the static stability of the structure. One approach is to bind the end modules together using a platform which can compensate for the tensile stresses and the outward movements.

The methodology presented for arches and vaults can be expanded to the design of supports. This can be achieved with a module-based interlocking anchoring foundation. Figure 10 shows a set of curves in red color corresponding to a hyperbolic vault along with the proposed base support generated using non-uniform rational b-spline (NURBS) curves shown in green color.

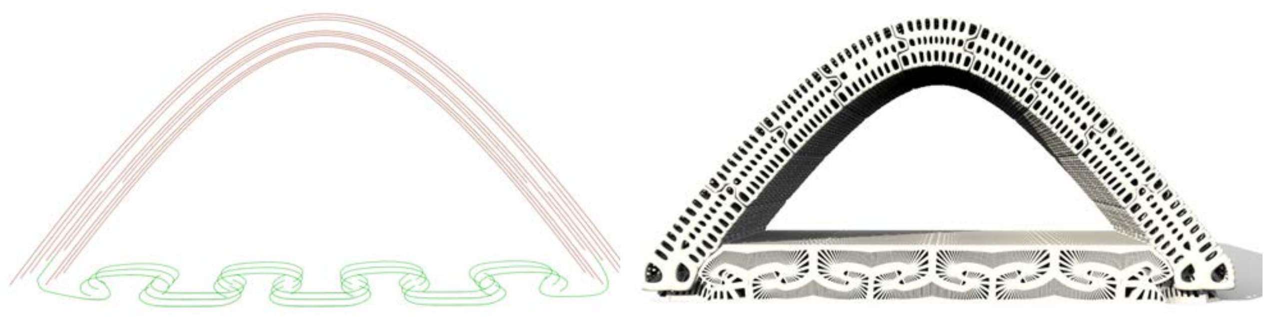

(a) *(b)*

Figure 10: *A hyperbolic vault and anchor support assembly generated using the novel method. (a) The nurbs curves for base support are shown in green color while the curves corresponding to the hyperbolic vault are shown in red color. (b) Resulting modules of the vault and anchoring assembly.*

For the design of the anchor support, three nurbs curves were spaced ¼ d distance apart expect in case of end support which has 1 nurbs curve. It is covered by the end module of the vault as displayed in Figure 10a and 11a. Also, during computation of the end modules of the hyperbolic vault, both the guide curves and interlock curves were translated according to Step 5 instead of Step 5 and 6 for simplification of the anchor support and assembly movement. The end support module forms one half of the module bound for the hyperbolic vault end module. Two possible solutions are been discussed in relation to this in Figure 11.

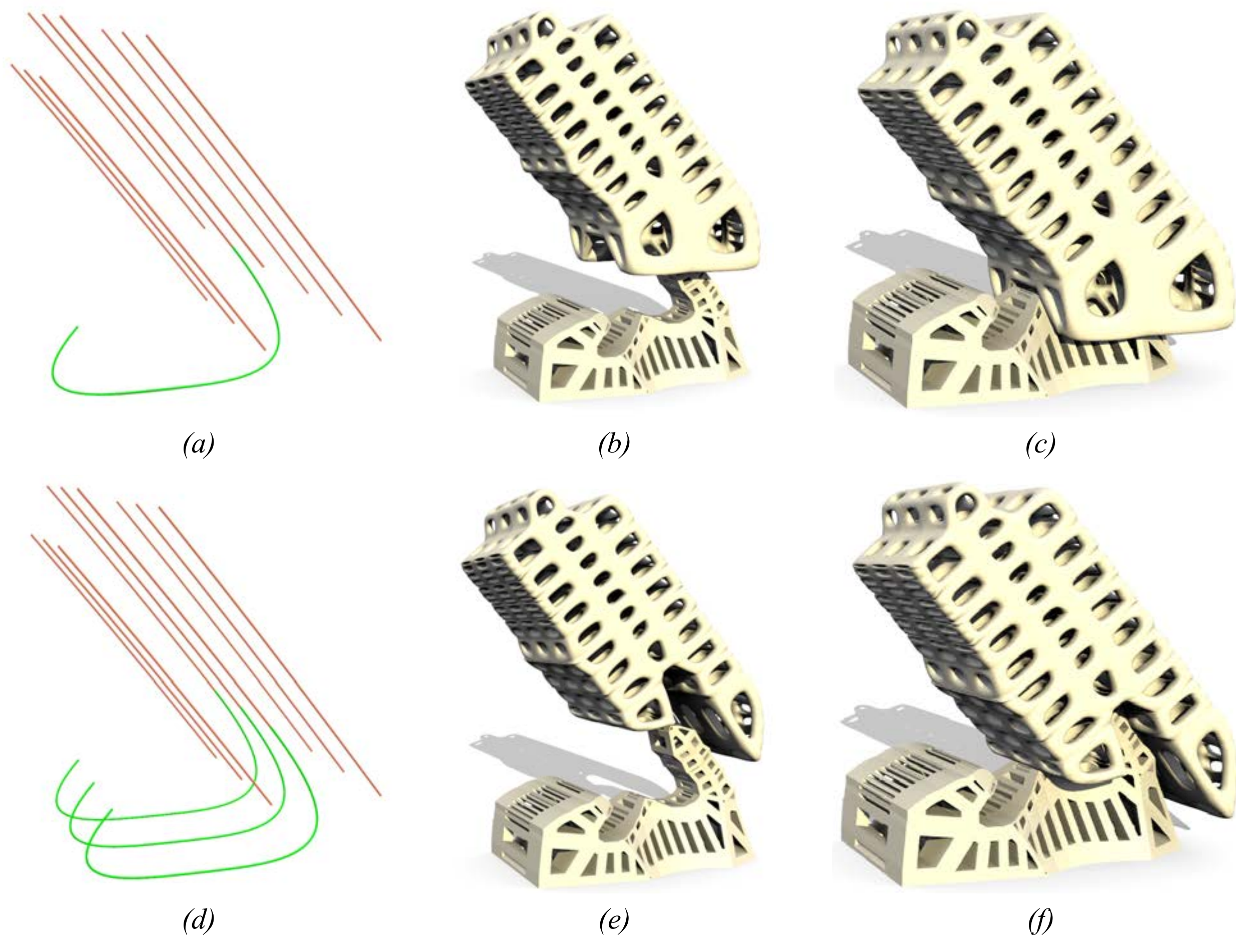

Figure 11: *End module design for the hyperbolic vault. (a) One green nurbs curve is included in the module bound of the hyperbolic vault end module for which the set of curves is shown in red color. (d) Three green nurbs curves are included in the module bound of the hyperbolic vault end module curve set shown in red color. (b) and (e) are corresponding depiction of the assembly movement. (c) and (f) show the final interlock of the support and vault module.*

The anchoring structure interlocks in XY plane but can slide in Z direction. Once in place, the tensile forces developed in the anchor support due to the vault will likely keep the anchoring modules from slipping out. However, a robust support system should be explored in future studies. The assembly for the anchor supports can be center outwards to end supports, while the assembly for arch or vault could be end modules upwards to the keystone. The interlock angle ø and the weight of the modules will determine if the modules need additional temporary support during construction. A potential assembly sequence is shown in Figure 12.

Figure 12: *Potential assembly sequence of an interlocking hyperbolic vault. The end module of vault and end modules of the support will be connected by movement in XY plane while all the rest of the module can be placed with a horizontal movement along the Z axis. Refer to Figure 1 for the coordinate system.*

Discussions

It is fairly obvious to state that the set of curves in 3D design domain are of crucial importance in determining the form and interlocking mechanism. However, the impact of decomposing the curves into points is also significant. During the decomposition of m_p module curves into i points, the endpoints are excluded because of coincidences with endpoints of adjacent m_{p-1} and m_{p+1} module curve set. As long as the curve decomposition to points is uniformly spaced, the Voronoi computation will ensure that the module cell boundary will overlap with the endpoints.

Decomposition of inner and outer vault bound curves into j points is crucial in determining the internal and external form of the module. For avoiding protrusions, radially project ¼ h arch decomposed points onto the inner bound curve and ¾ h arch points onto outer bound curve. Otherwise, the decomposition can be independent of the module curve decomposition and result in protrusions depending on the i and j parameters. Later will result in a wide range of module shape which can be adjusted according to the design intent. Ideally, increasing the number of i and j points will result in a smoother and uniform surface but also increase the computation expense associated with the solution set. Also, currently the method incorporates all the points of the neighboring modules, and vault bound. This is carried out to account for the possibility of complex free form curves, however, only nearest 400 points from the bounding point collection b_p are considered during the Voronoi computation for each seed point in the collection s_p. The form of each seed point's Voronoi cell is affected drastically by the initial 20-50 points and usually minor adjustments are noted after that. 400 nearest points were selected to balance the form and computation expense.

The method presents a generic approach to develop interlocking assemblies of arches and vaults. However, there are additional adjustments that need to be accounted for, especially in case of end modules, as discussed in relation to Figure 11. Also, the flexibility to generate repetitive modules gets limited if the angle made by the module, $\frac{\pi}{q}$ in case of semicircular arches, changes non-uniformly relative to the curve length, for instance in case of parabolic or hyperbolic vault. This is something to be explored in future studies. Another possible variation of the algorithm could be to vary the angle made by the modules in semicircular arches and vaults itself. For instance, Figure 7 and Figure 13 are similar on all the major parameters mentioned in the methodology. However, in Figure 7 all guide curves formed equal angle at the center of the circle ($\frac{\pi}{7} \sim 25.71^{\circ}$) whereas in Figure 13 the keystone guide curve angle (30º) is different than the rest of the guide curve angles (25º). This in turn changes the eventual form of the arch and should be considered as another parameter and tool in the future studies.

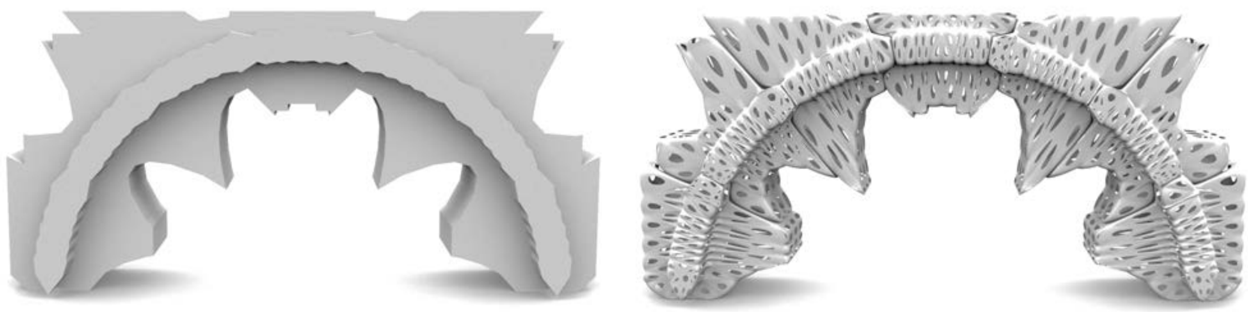

Figure 13: *An interlocking arch symmetric about the center keystone with keystone guide curve forming a larger angle at the center (30º) as compared to the rest of the modules (25º) . (Left) Union of all modules; (Right) Arch assembly with porous modules. {Parameters: $n = 1$, $d = 3$, $r = 7$, $h = 2$, $q = 9$, $\o = 3^{o}$, $i = 8$, and $j = 7$}*

Meanwhile, interlocking arches similar to Figure 6 can be useful in exploring modified versions of modules. Figure 14 below shows one such modification. The original module in 14a was obtained after a low *j* count of vault bound. The use of Kangaroo Physics, a physics-based plugin for Grasshopper, was utilized to turn the edges into spring-based systems [12]. The interlocking edges were fixed along with some additional desired edges while the rest of the surface was allowed to reach an equilibrium state. This effectively provide one solution to retain the interlocking properties and getting rid of any unwanted protrusions as seen in 14b. The complete assembly with the modified module and original keystone module is shown in 14c.

(a) *(b)* *(c)*

Figure 14: *(a) Original porous module obtained by the proposed methodology {Parameters: $n = 1$, $d = 3$, $r = 7$, $h = 2$, $q = 7$, $\o = 5^{o}$, $i = 5$, $j = 18$}. (b) Modified porous modules after the use of spring-based system to get rid of unwanted protrusions while preserving the interlocking edges. (c) Interlocking semicircular arch assembly with six modified porous modules and one original keystone modules*

While this paper has presented evidence that the method can be used to generate a wide range of interlocking arch and vault assemblies, there is tremendous scope for future applications. Interlocking domes should be explored in the next phases along with evaluations of the structural performances of the geometric forms. Meanwhile, additional studies on various interlocking patterns and weaving techniques, especially those utilizing Voronoi tessellation-based form generation, should be utilized to enhance stability of the interlocking structures in the future [13]. Examining the role of the interlock angle ø in supporting the arch during construction sequence can be another objective for future studies.

Conclusion

This paper presented a novel method to generate interlocking arches and vaults by Voronoi decomposition of 3D space using curves. It was demonstrated to work with semi-circular arcs, hyperbolic segments and nurbs curves. Additive manufacturing was utilized for fabricating interlocking arch modules, and conceptual extension to anchor support structure was also explored. The method is likely to provide architects and designers a powerful tool to generate interlocking structures while presenting adequate scope for future research and practical applications.

Acknowledgements

I would like to acknowledge that this work is a result of many stimulating discussions and collaborations over the past few years. Special thanks to Ergun Akleman, Julian Kang, and Wei Yan. I would also like to thank the reviewers for their constructive feedback towards improving the manuscript.

References

[1] R. Decastes. *Principia Philosophiae*. 1644

[2] G. L. Dirichlet. "Über die Reduktion der positiven quadratischen Formen mit drei unbestimmten ganzen Zahlen." *J. reine angew. Math.* vol. 40, 1850, pp. 209-227.

[3] G. Voronoi. "Nouvelles applications des paramètres continus à la théorie des formes quadratiques." *J. reine angew. Math.* vol. 133, 1907, pp. 97-178.

[4] A. Borhani and N. Kalantar. "APART but TOGETHER - The Interplay of Geometric Relationships in Aggregated Interlocking Systems." Proceedings of the 35th eCAADe Conference, vol. 1, 2017, pp.639-648.

[5] G. Fallacara (2006). "Digital stereotomy and topological transformations: reasoning about shape building." Proceedings of the second international congress on construction history, vol. 1, 2006, pp. 1075-1092.

[6] S.G. Subramanian et al. "Delaunay Lofts: A biologically inspired approach for modeling space filling modular structures." *Computers & Graphics*, vol 82, 2019, pp. 73-83.

[7] E. Akleman et al. "Generalized Abeille Tiles: Topologically Interlocked Space-Filling Shapes Generated Based on Fabric Symmerties. *Computers & Graphics*, 2020.

[8] McNeel and Associates. "Rhinoceros3D". https://www.rhino3d.com

[9] E. Catmull and J. Clark. "Recursively generated B-spline surfaces on arbitrary topological meshes." *Computer-Aided Design,* vol. 10, 1978, pp 350-355.

[10] Shenzhen Creality 3D Technology Company, Limited. "Ender 3 3D Printer". https://www.creality3dofficial.com/products/official-creality-ender-3-3d-printer

[11] Ultimaker. "Ultimaker Cura 4.2.1". https://ultimaker.com/software/ultimaker-cura

[12] D. Piker. "Kangaroo Physics". https://www.food4rhino.com/app/kangaroo-physics

[13] V.R. Krishnamurthy et al. "Bi-Axial Woven Tiles: Interlocking Space-Filling Shapes Based on Symmetries of Bi-Axial Weaving Patterns." 46th Annual Graphics Interface Conference, 2020.